Journal of Non-Crystalline Solids 355 (2009) 2496–2502

Contents lists available at ScienceDirect

Journal of Non-Crystalline Solids

journal homepage: www.elsevier.com/locate/jnoncrysol

Trapping organic molecules in sol–gel aluminosilicate matrices

O. Martínez-Zapata [a], J. Méndez-Vivar [a,*], P. Bosch [b], V.H. Lara [a]

[a] Universidad Autónoma Metropolitana-Iztapalapa, Depto. de Química A. P. 55-534 México, D. F. 09340, Mexico
[b] Instituto de Investigación en Materiales, Universidad Nacional Autónoma de México Circuito Exterior s/n, Ciudad Universitaria, D. F. 04510 México, Mexico

ARTICLE INFO

Article history:
Received 28 November 2008
Received in revised form 30 June 2009
Available online 24 September 2009

PACS:
81.20.Fw
82.33.Ln
81.05.−t
81.05.Rm

Keywords:
Chemical properties
Ion exchange
Diffraction and scattering measurements
X-ray diffraction
Measurement techniques
Optical spectroscopy
Scanning electron microscopy
Microstructure
Porosity
Powders
Optical properties
Absorption
Oxide glasses
Aluminosilicates
Sol-gel, aerogel, and solution chemistry
Sol–Gels (xerogels)
X-rays

ABSTRACT

Inorganic materials may be tailored to obtain specific pore size distributions and surface structures. In this work we present the synthesis of faujasite type amorphous aluminosilicate matrices by the sol–gel process. One of the preparations included the use of mesitylene as a template to create additional porosity. The powders were used to encapsulate the dyes methylene blue (MB) and malachite green (MG). Several analysis were performed, including X-ray diffraction (XRD), small angle X-ray scattering (SAXS), nitrogen adsorption/desorption, scanning electron microscopy (SEM), UV–vis, and diffuse reflectance spectroscopy. According to the results, MB and MG were effectively trapped in the aluminosilicate matrix.

1. Introduction

The understanding of the adsorption processes is very important in the design and preparation of adsorbents for specific molecules [1]. Surface functionalization is also helpful to improve the adsorption capacity and selectivity of the adsorbents by taking advantage of specific interactions between adsorbents and adsorbates, the porosity and the textural properties [2–4].

The sol–gel technique can be exploited to tailor inorganic materials with specific properties such as regular cavities to perform as molecular sieves, trapping organic molecules with commercial value at low temperature [5–8]. Among those materials the aluminosilicates are particularly interesting for that purpose because they possess big pore volumes, suitable to encapsulate organic molecules [9–12].

In the present research we developed an experimental procedure to obtain and characterize amorphous aluminosilicate, via the use of alkoxides of Si, Al, and Mg and using an aqueous solution of NaOH. This latter reagent served as a basic catalyst. Simultaneously the Na cations were incorporated into the matrix and then, we used the amorphous aluminosilicate for trapping organic molecules. The dye molecules used were 4-[(4-dimethylaminophenyl)-phenylmethyl]-*N*,*N*-dimethylaniline (malachite green, MG) and 3,7-bis(dimethylamino)phenazathionium chloride (methylene blue, MB). Both of them are cationic species, soluble in water and 2-butanol. They also exhibit high molar extinction coefficients. Previous studies performed by other researchers have shown that

* Corresponding author. Tel.: +52 55 5804 6543; fax: +52 55 5804 4666.
E-mail address: jmv@xanum.uam.mx (J. Méndez-Vivar).

0022-3093/$ - see front matter © 2009 Elsevier B.V. All rights reserved.
doi:10.1016/j.jnoncrysol.2009.08.021

cationic dye molecules can be incorporated in the cavities of crystalline aluminosilicates, either by ion exchange or during crystallization [13–15]. As silanol has a negative charge, we believe that the organic cations will be effectively incorporated into the silica. Therefore, we used methylene blue (C. I. – 52 015) and malachite green (C. I. – 42 000B), which are widely used as oxidation–reduction agents, to stain in bacteriology and to dye silk, wool, cotton, etc. [16].

The goal of this research was to synthesize amorphous aluminosilicates by the sol–gel process, with pore volumes appropriate to encapsulate the dyes MG and MB. According to our results when the dyes were impregnated to the obtained materials, they could be trapped in the internal structure of the matrix. We performed several spectroscopic analyses that demonstrated this.

UV–vis and diffuse reflectance spectra of the dye-impregnated adsorbents are employed to confirm the incorporation of MB an MG into the amorphous aluminosilicate.

2. Experimental

2.1. Synthesis of the aluminosilicate

The following procedure describes the preparation to obtain 5 g of an aluminosilicate with the typical composition of a faujasite X, via the sol–gel process: 2.5×10^{-4} mol of tetraethyl orthosilicate (TEOS, 98 wt%, Aldrich) dissolved in 2-butanol (2-BuOH) was slowly mixed in a round bottom flask with 1.0×10^{-4} mol of magnesium methoxide (MMg, 9.8 wt%, Aldrich) at room temperature. 9.4×10^{-5} mol of aluminum tri-*sec*-butoxide (T*sec*BuAl, 97 wt%, Aldrich) was added by dropping. An aqueous NaOH (98.5 wt%, J. T. Baker) solution containing 1.2×10^{-4} mol of NaOH was also added by dropping. The cloudy sol gradually produced was refluxed at 353 K during seven hours. The resulting suspension was filtered by gravity and washed with 30 mL 2-BuOH. The powder was left to dry at room temperature during 12 h and later on in an oven at 523 K during 24 h in air atmosphere.

2.2. In situ trapping of the dyes

The incorporation of a 1.0 mol% solution of the dyes 4-[(4-dimethylaminophenyl)-phenylmethyl]-*N*,*N*-dimethylaniline (malachite green, MG) or 3,7-bis(dimethylamino)phenazathionium chloride (methylene blue, MB) in 2-BuOH was done separately, right after adding the NaOH solution to the reacting mixture (see above paragraph). The molecular structure of the dyes can be seen in Fig. 1. The drying temperature of the gels obtained was chosen to be lower than the decomposition temperature of the dyes in order to corroborate that the dyes were effectively trapped in the aluminosilicate matrix. In this way, the drying temperature was 443 K, knowing that the decomposition temperatures for MG and MB are 465 and 463 K, respectively.

2.3. Incorporation of an organic template into the matrix

1,3,5-Trimethylbenzene (mesitylene ME, 98 wt%, Aldrich) was incorporated to the reacting mixture in order to create additional porosity in the final solid and intending to enhance the encapsulation of the dyes; see Fig. 2 [17]. The mesitylene content was 10.0 wt%. The gel obtained was left to dry, first at room temperature (293 K) and later on during 24 h in air atmosphere at 443 K. In this case the dye trapping was done spreading a small amount of the modified aluminosilicate as a dry powder over a solution containing the dye in a concentration 3.5×10^{-4} M, while stirring at room temperature.

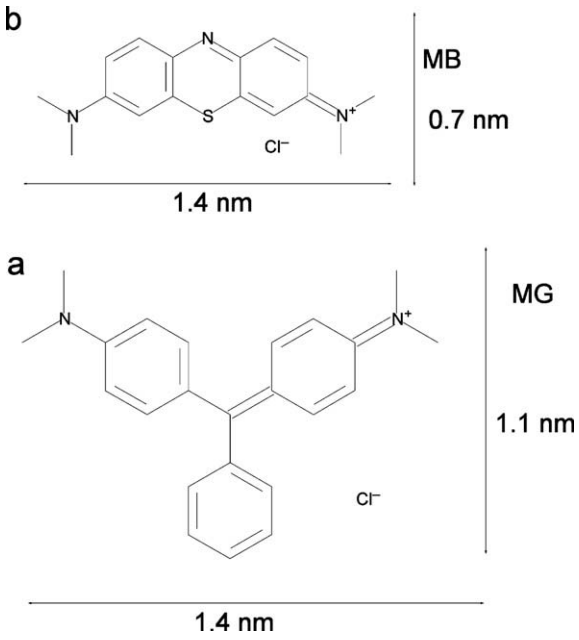

Fig. 1. Molecular structure and size of the dyes: (a) 44-[(4-dimethylaminophenyl)-phenylmethyl]-*N*,*N*-dimethylaniline (malachite green) and (b) 3,7-bis(dimethylamino)phenazathionium chloride (methylene blue). The sizes were estimated using the program GaussView2.0.

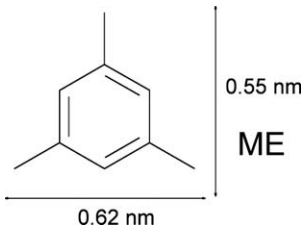

Fig. 2. Molecular structure and size of 1,3,5-trimethylbenzene (mesitylene) estimated with the program GaussView2.0.

2.4. Characterization

The X-ray diffraction patterns were obtained using a siemens D500 diffractometer with CuKα radiation (λ = 1.5406 Å) and a diffracted beam monochromator. Compounds were identified in the conventional way using the JCPDS files.

Radial distribution functions were obtained from X-ray diffraction patterns measured with a molybdenum anode tube, only in this way it was possible to reach the required high values of the angular parameter. These diffractograms were the input data for the radiale program [18].

Small angle X-ray scattering (SAXS) experiments were performed using a Kratky camera coupled to a copper anode tube whose K-α radiation was selected with a nickel filter. The collimated X-ray beam was linear and corresponded to an 'infinitely high' beam. The SAXS data, collected with a proportional linear counter, were processed with the ITP program [19–22] where the angular parameter, h in Å^{-1}, is defined as $h = (4\pi\sin\theta)/\lambda$, where θ and λ are the scattering angle and the X-ray wavelength, respectively. Measurement time was 9 min in order to obtain acceptable statistic results.

The shape of the scattering objects was estimated from the Kratky plot; i.e. $h^2I(h)$ vs h. From this plot it is possible to assess if the shape is fibrillar or globular. If the Kratky curve presents a broad

peak, the scattering objects most probably present a globular conformation whereas if the curve approximates a plateau the particles most probably are fibril-like objects [23,24]. Once the shape is known it is possible to calculate the distance distribution functions [21]. Still, the Log $I(h)$ vs Log h plot provides the fractal dimension [25–27].

The sample X was analyzed in a quantachrome autosorb automated gas sorption system to obtain the nitrogen adsorption isotherm at 77.4 K. The specific surface area was estimated with the Brunauer–Emmett–Teller (BET) model and the pore size distribution was evaluated with the BJH model. All samples were outgassed at 573 K for 1 h prior to analysis.

A Leica Stereoscan 440, scanning electron microscope (SEM) was used. The samples had to be previously covered with a layer of gold in order to prevent charge problems. Only two samples (XMEMB and XME) were studied with this technique.

UV–vis spectra were obtained on a Lambda 40 Spectrometer using 2-butanol as solvent. The diffuse reflectance measurements were done using the labsphere RSA-PE-20 accessory. In this latter case the samples were diluted with $BaSO_4$ before the study. In all cases the spectra were recorded in the 400–800 nm region.

3. Results

3.1. X-ray diffraction (XRD)

Three conventional X-ray diffraction patterns are compared in Fig. 3. This figure has the purpose of showing that although an incipient crystalline structure is observed in sample X (Fig. 3(a)), as shown by the weak peak al 12° (2θ), this aluminosilicate is not crystalline as it presents a broad peak from 10° to 40° (2θ). The sample XMEMG (Fig. 3(b)) did not show the weak peak located at 12° in Fig. 3(a). No crystalline compounds could be identified. The X-ray diffraction pattern of crystalline MG is included for comparison purposes (see Fig. 3(c)).

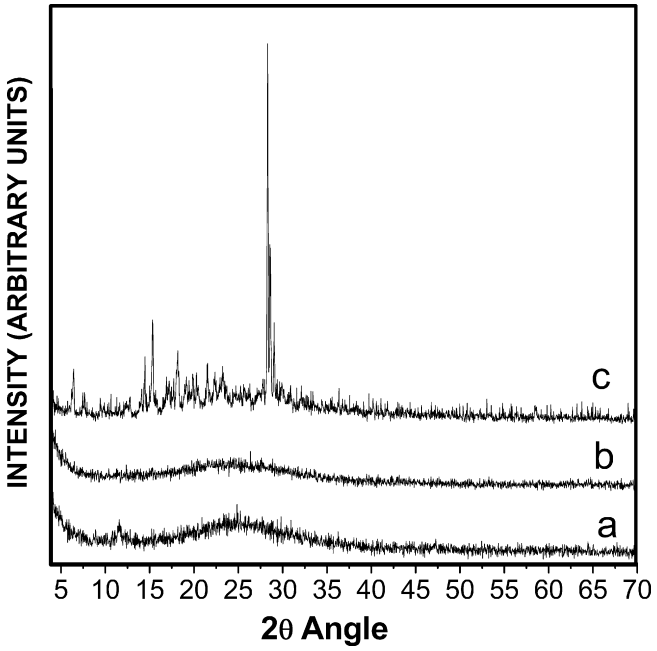

Fig. 3. X-ray diffraction patterns: (a) pure amorphous aluminosilicate dried at 523 K (sample X), (b) sample X prepared using mesitylene to create additional porosity and later on impregnated with malachite green. The sample was dried at 443 K (sample XMEMG), and (c) malachite green (MG).

3.2. Radial distribution functions (RDF)

The radial distribution functions were determined to find out if there was some short range order. In Fig. 4(a) (Sample X dried at 523 K) the first peak appears at a radial distance of 0.17 nm and the second at $r = 0.23$ nm. These two distances correspond to T–O and O–O bonds, respectively [28,29], where T is a Si or Al atom in the tetrahedral building unit of the aluminosilicate. It has to be emphasized that the distance Mg–O is 0.21 nm and therefore it is included in the peak at 0.23. The third peak, appearing at a radial distance of 0.34 nm, can be attributed to a T–T distance. This distance defines the average angle between adjacent tetrahedra which we estimated to be *ca.* 180°; see Fig. 5(a). Thus, the material is constituted by chains of SiO_4 tetrahedra. The second neighbors T–O, T–T, and O–O produce the following peaks at 0.44 and 0.50 nm. These peaks differ from those reported by other authors for amorphous SiO_2 [30]: Si–O = 0.16, O–O = 0.27, and Si–Si = 0.32 nm. The distance Mg–O is the same as the distance O–O and therefore Mg is incorporated to the aluminosilicate matrix.

When the previous radial distribution function is compared to sample XMG (see Fig. 4(b)), the first neighbor distances are reproduced, as expected. They correspond to the tetrahedra which are

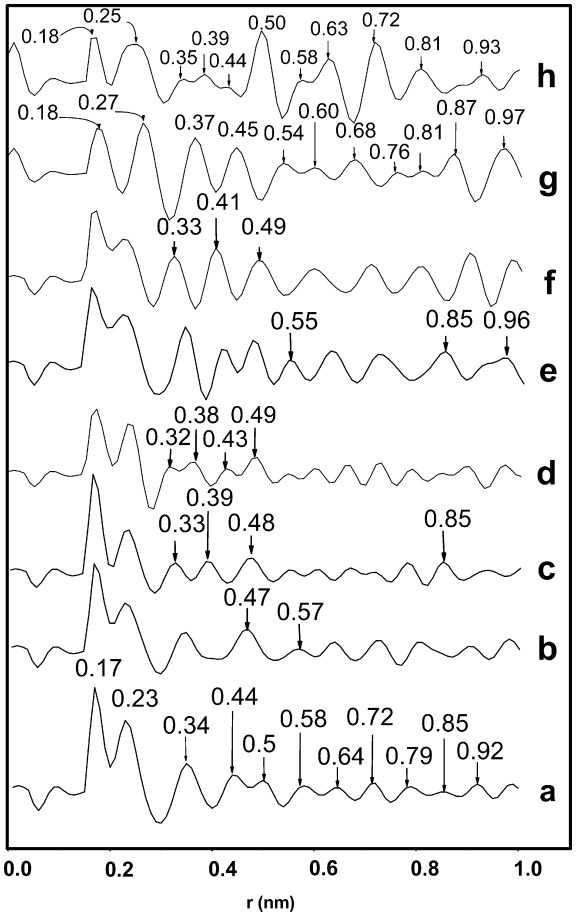

Fig. 4. Radial distribution function results of samples dried in air 24 h: (a) amorphous aluminosilicate (sample X) dried at 523 K, (b) sample impregnated with malachite green (sample XMG) dried at 443 K, (c) sample prepared using mesitylene, and later on impregnated with malachite green (sample XMEMG) dried at 443 K, (d) sample prepared using mesitylene (sample XME) dried at 523 K, (e) aluminosilicate impregnated with methylene blue (sample XMB) dried at 443 K, (f) sample prepared using mesitylene impregnated with methylene blue (sample XMEMB) dried at 543 K, (g) malachite green (MG), and (h) methylene blue (MB). The accuracy of the calculations was $\pm 1 \times 10^{-2}$.

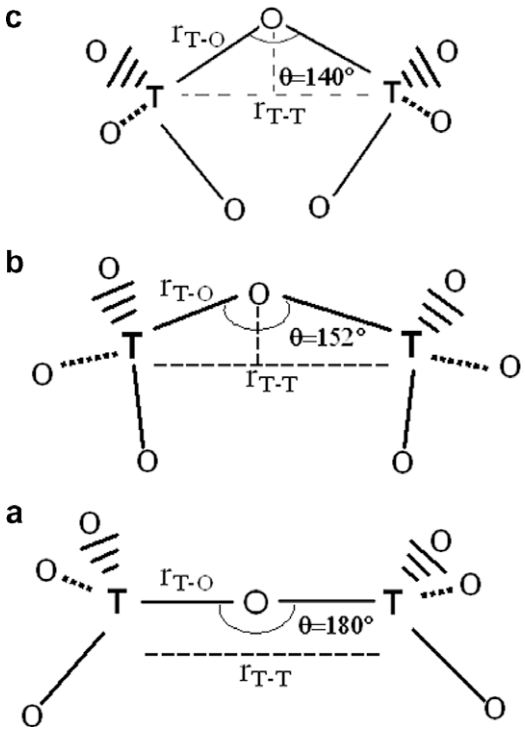

Fig. 5. Schematization of T–O–T (T: Si, Al) angles calculated between adjacent tetrahedral, from information derived from the radial distribution function results: (a) 180°, (b) 154°, and (c) 140°.

not altered by the dye incorporation. Furthermore, the T–T peak at 0.34 nm is not shifted, showing that the angle between the tetrahedra is not modified. The only difference is that the second neighbor peaks at 0.44 and 0.5 nm are no more resolved and constitute a single peak at 0.47 nm which can also be attributed to MG. Indeed, crystalline MG has a peak at 0.45 nm (see Fig. 4(g)). Hence, the 0.47 nm peak is the result of the combination of the MG peak and those of the support. Thus, the dye molecules are, to a very low extent, dispersed in the aluminosilicate. Note that the radial distribution function of the dye presents well defined and intense peaks even at radial distances of 1.0 nm showing that the compound is crystalline. The distances due to the dye molecule do not alter the short range order (distances less than 0.3 nm) as they are similar to the T–O and O–O bonds, so, if they are present they are not resolved. From these results we conclude then, that the dye molecules are occluded in the interstitial cavities of the aluminosilicate matrix.

Comparing the sample XMG to XMEMG (see Fig. 4(b) and (c), respectively) the differences between them is that the sample corresponding to the latter one had been prepared using mesytilene as a template. Fig. 4(c) presents the same two peaks as Fig. 4(b), which were attributed to T–O and O–O distances present in the TO_4 tetrahedron. The following peaks in Fig. 4(c) are found at 0.33, 0.39, and 0.48 nm. Hence the T–T peak is shifted to a lower value (being now 0.33) showing that the angle between tetrahedra has been lowered and is now *ca.* 152°; see Fig. 5(b). The structure has become denser or is affected by some other compound whose distances superimpose onto those of the aluminosilicate. The 0.39 and 0.48 nm peaks can be correlated to the radial distribution function of the crystalline MG dye (Fig. 4(g)) which presents peaks at 0.37 and 0.45 nm. Therefore, the dye could form crystalline agglomerates into the aluminosilicate matrix whose size could be larger than 2.0 nm in diameter as the crystalline dye peak at a radius of 0.85 nm is present in Fig. 4(c).

In Fig. 4(d) (sample XME) the results obtained for the amorphous aluminosilicate where mesytilene was used as a template to enhance the porosity in the matrix can be seen. The sample turned out to be brownish after drying in air for 24 h at 523 K. The appearance can be attributed to organic residues from mesytilene. As in Fig. 4(c), the first two peaks, up to $r = 0.3$ nm reproduce the order found in the original aluminosilicate. The third and fourth maxima are located at $r = 0.32$ and 0.38 nm. Again the matrix structure is either distorted to an angle of *ca.* 140° (see Fig. 5(c)) or the bonds of residual mesytilene are superimposed, or both. The T–O and T–T second neighbors, are now 0.43 and 0.49 nm.

The radial distribution function in Fig. 4(e) (sample XMB) exhibits as main features peaks at 0.35 nm and 0.55 nm that cannot be attributed to MB (Fig. 4(h)). Although these peaks were already found in Fig. 4(a) (sample X, the matrix) they are much more intense. Then, most probably they are also due to bonds between the dye molecule and the matrix in a very strong interaction. Intense peaks at 0.85 and 0.96 in Fig. 4(e) were not found in the matrix nor in the crystalline MB. The radial distribution function of Fig. 4(f) (sample XMEMB) is similar to the curve of pure aluminosilicate up to $r = 0.33$ nm. At 0.41 nm, a clearly defined peak appears which can be attributed to the MB molecule trapped in the matrix; see Fig. 4(h). According to these results the amorphous network is distorted due to the presence of other compounds such as organic residues derived from mesytilene. The peak at 0.49 nm is the unresolved distance due to (Si, Al)–O and (Si, Al)–(Si, Al), second neighbors, but it can also be assigned to methylene blue; see Fig. 4(h). The peaks present in MB up to $r = 0.72$ nm appear in this sample. Again, small crystalline dye clusters are occluded in the matrix.

3.3. Small angle X-ray scattering (SAXS)

The aluminosilicate used as matrix presents a fractal dimension of 2.9 (figure not shown here) The Kratky plot is typical of a lamellar shape as in all the other samples. The scattering objects in this case are pores as they are altered by the dye adsorption. The corresponding size distribution of sample X presented in Fig. 6(a) is broad and the maxima are located at $r = 9.9$ and 11.1 nm. The MG affects the fractal dimension whose value was reduced to 2.5. The corresponding size distribution turns out to be monomodal with a maximum at 7.5 nm in sample XMG; see Fig. 6(b). We assume that the dye molecules, fill the large and the small matrix pores. Indeed, the dye molecule sizes are between 0.7 and 1.4 nm; see Fig. 1. As a consequence the resulting pore size distribution is now centered at a radius of 7.5 nm.

The fractal dimension and pore shape of sample XMEMG are the same as in the previous sample. The incorporation of mesitylene gives as a result a shoulder at 10.8 nm in Fig. 6(c). Apparently, residual mesitylene inhibits the adsorption of malachite green into the largest pores and facilitates the diffusion into the smaller pores of the matrix.

The sample XME corresponding to Fig. 6(d) exhibits a fractal dimension of 2.2 and also a lamellar pore shape. The corresponding pore size distribution presents a maximum at $r = 2.1$ nm and a secondary maximum at 4.5 nm. Pores are filled and a two modal pore size distribution is produced. The mesitylene molecules have been completely eliminated from the matrix, as the sample was dried at a higher temperature (523 K), compared to Fig. 6(c) (443 K). The corresponding fractal dimension value of the impregnated matrix (sample XMB) is 2.3; see Fig. 6(e). The maxima in the pore size distribution are at 1.8, 3.9, 6.6, and 9.9 nm. Apparently, the MB molecules occupy mainly the largest cavities, which was expected. The pore shape and pore size distribution in

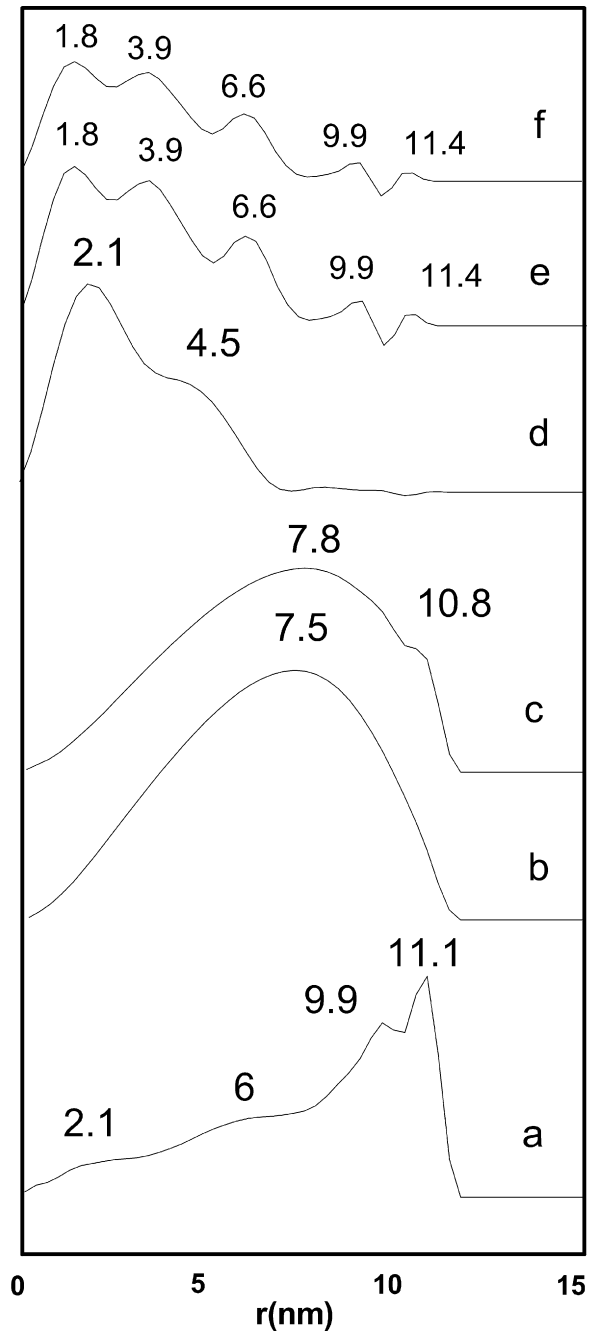

Fig. 6. Pore size distribution calculated from SAXS measurements of samples dried in air 24 h: (a) X (523 K), (b) XMG (443 K), (c) XMEMG (443 K), (d) XME (523 K), (e) XMB (443 K), and (f) XMEMB (443 K).

Fig. 6(f) (sample XMEMB) reproduces the values reported for the previous sample (Fig. 4(d)).

3.4. Nitrogen physisorption

Fig. 7(a) shows the nitrogen adsorption–desorption isotherm of the sample X. The shape corresponds to a type IV isotherm according to the IUPAC classification [31,32]. The hysteresis loop can be attributed to the presence of open pores where no condensation is evident; therefore ink bottle shaped pores have to be discarded. According to these results the pore size varies between 5 and 9 nm diameter (see Fig. 7(b)). The corresponding surface area was 170.1 ± 1.4 m^2/g.

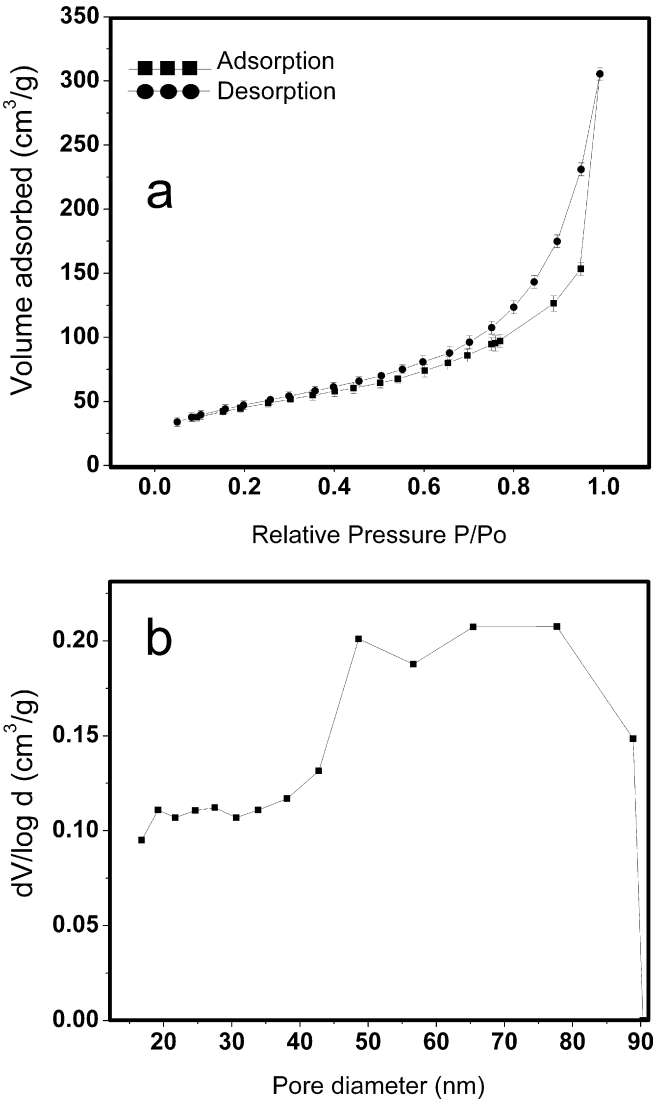

Fig. 7. (a) Nitrogen adsorption/desorption isotherm of sample X at 77.4 K, (b) BJH pore size distribution.

3.5. Scanning electron microscopy (SEM)

In order to understand the mesitylene effect the samples XME and XMEMB were studied by SEM. Fig. 8 compares the corresponding micrographs. The particles are more ordered and similarly oriented in the XMEMB sample (Fig. 8(b) and (d)), where pores are lamellar. The observed lamellar shape of pores determined by SAXS at a nanometer scale is then confirmed by SEM. Still, both samples present very large and dense agglomerates beyond the SAXS resolution.

3.6. Diffuse reflectance and UV–vis spectroscopy

The experimental UV–vis spectrum of a MB 3.9×10^{-4} M solution is shown in Fig. 9(a). A strong band appears at 652 nm and a shoulder at 603 nm, both corresponding to MB as a monomer. In the diffuse reflectance spectrum of X impregnated with MB (figure not shown here) a wide band appears at 611 nm. This band is assigned to the formation of the so-called H-aggregates (dimers, trimers, and oligomers) [33].

The UV–vis spectrum of a MG 3.9×10^{-4} M solution appears in Fig. 9(b). A strong band appears at 622 nm and a shoulder at

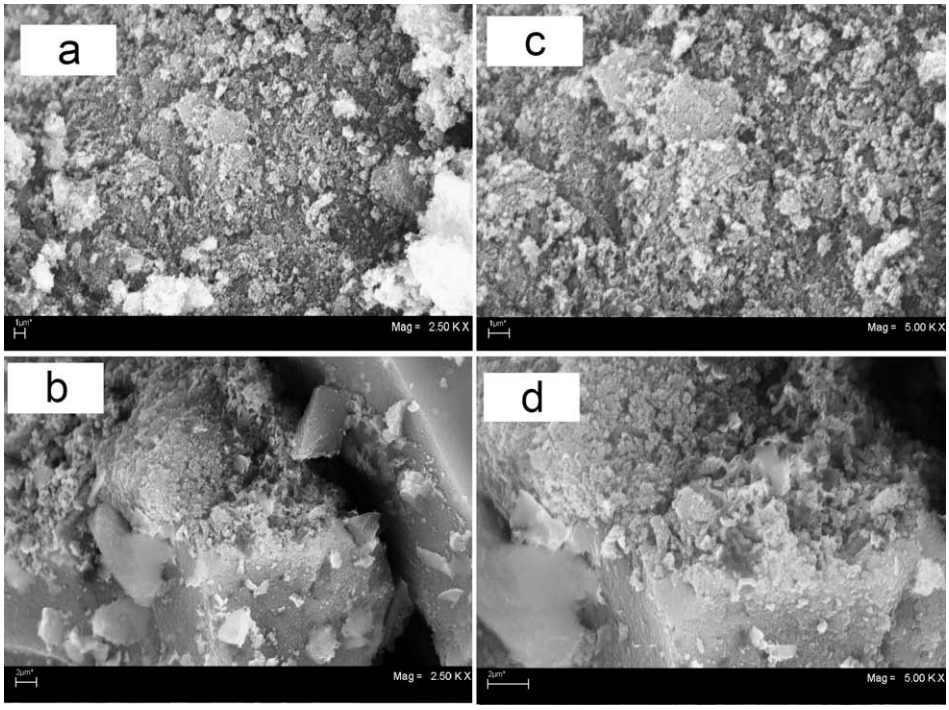

Fig. 8. Scanning electron microscopy (SEM) results of samples magnified 2.5 K: (a) XME (523 K) and (b) XMEMB (443 K). Samples (c) XME (523 K) and (d) XMEMB (443 K) were magnified 5 K.

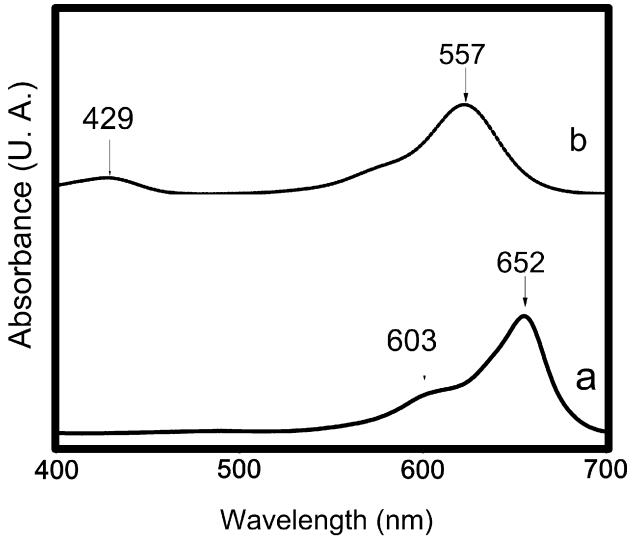

Fig. 9. (a) UV–vis spectrum of a MB 3.9×10^{-4} mol solution, (b) UV–vis spectrum of a MG 3.9×10^{-4} mol solution.

557 nm. A weak band also appears at 429 nm. The corresponding diffuse reflectance spectrum of X impregnated with MG solution gave as a result a spectrum (not shown here) where a single band appears at 617 nm. Föster in Ref. [34] attributed this result to the formation of deprotonated MG dimers deposited on the surface of the solid.

4. Discussion

The matrix is a flexible network of silicon tetrahedra linearly assembled forming layers. Between the layers, two dimensional pores are found which are accessible to gases. This reasoning is supported by the N_2-isotherm results. Then, clusters of dye molecules can be storaged. When a template is used, the angle between tetrahedra is modified as can be seen in Fig. 5. Considering that MB molecules are rigid structures, they could interact with the surface matrix through one end (if the molecules were lying parallel to the surface matrix, the fractal dimension would not be significantly altered), and the interaction zone is localized. These results agree with those of the UV–vis and diffuse reflectance studies. Instead, MG molecules can be considered as flexible structures, having an electric charge more homogeneously distributed. The resulting contact surface could be large, and the resulting interaction between MG and the matrix could be weaker. Summarizing, the interaction between MB and the matrix is stronger compared to the interaction between MG and the matrix. Such interaction is revealed by the changes in the fractal dimension. Such results have to be discussed considering the main features of the matrix first and then the size and shape of the cationic molecules. The layers of the matrix may be described as weakly cross-linked chains in two dimensions. Then, two types of surface could be present, the planar and the edge surfaces.

Dye molecules are small enough to occupy the pores as it was concluded from the pore size distributions from SAXS. It has to be emphasized that the dye impregnation was made on the matrix containing organic residues. MG occupies smaller pores than MB as the small pores present in the pore size distribution of sample X disappear in the first case with impregnation and only large pores are observed. Both molecules have similar approximate sizes but their shape is different; MG can be said to be globular and MB seems to be an elongated cylinder. The different location of the molecules in the various pores cannot be explained just as a result of a sterical effect. There is an effective electronic interaction between the pore walls and the molecule. In some cases dye molecules may agglomerate to constitute large entities which could not enter into the matrix pores.

MG diffuses better into the pores and reaches the bottom of the smaller ones whereas MB is anchored in the large pores; i.e., it does

not diffuse as its electric charge is located at the end of the linear molecule (MB). In MG the same charge can be delocalized throughout the molecule; see Fig. 1. It may also be interesting to refer here to the adsorption phenomena observed in other lamellar compounds, such as clays. In these minerals the adsorption on pore edges is often reported [35]. The adsorption on the broken edges can occur through a ligand exchange mechanism. The adsorbed species displace OH– from the surface and form partly covalent bonds with the structural cations. Such mechanism could explain that MB does not diffuse and is retained in the pore mouths where broken edges are found.

It is not possible to distinguish in the radial distribution function results the Si–O and Al–O distances, nor to determine the aluminum location. Hence it is not clear if aluminum is segregated or if it is homogeneously distributed in the solid. This remark is crucial as aluminosilicates, strong solid acids [36] have been reported to show a high ability for the sorption of basic dyes [37]. In a previous work [38] on adsorption of Basic Blue 41 on clays it was reported that the mechanism behind the dye adsorption involves the formation of H-aggregates of the dye on bentonite and montmorillonite. Time-dependent absorbance spectra revealed the presence of various dye species in montmorillonite. If molecules interact with each other, small clusters larger than 7.0 nm may be formed. These agglomerates cannot enter into the matrix mesoporous network. Hence, in our study two kinds of interaction could occur. On the one hand, isolated dye molecules enter into the matrix porous lattice interacting with acid centers and on the other, molecules interacting with each other constitute micelles which are weakly adsorbed on pore mouths. Thus, as MB molecule does not penetrate the matrix at the same extent as the MG does, MB molecules associate much more than MG molecules.

5. Conclusions

We developed a procedure to obtain faujasite type amorphous aluminosilicates by the sol–gel process. The porous structures were designed *ad hoc* to host the cationic dyes methylene blue (MB) and malachite green (MG). The porous structure was also modified in some cases using mesitylene as a template. The incorporation of the template gave as a result a distortion in the T–O–T angle as it was demonstrated by calculations from the radial distribution results.

We found important differences in the impregnation between MB and MG that can be attributed to sterical and charge distribution effects of these molecules. According to the results MG has a larger affinity to the matrix and can be easily incorporated. These findings can be used to contribute to the design of porous solids to clean contaminated streams with residual dyes coming out from industries.

Acknowledgments

The technical support of Dr Jose Guzman in scanning electron microscopy and financial support from CONACYT are gratefully acknowledged. O. Martínez-Zapata acknowledges a fellowship provided by CONACYT.

References

[1] G. Schulz-ekloff, D. Wöhrle, B.V. Duffel, R.A. Schoonheydt, Micropor. Mesopor. Mater. 51 (2002) 91.
[2] Z. Wu, L. You, H. Xiang, Y. Jiang, J. Colloid Interf. Sci. 303 (2006) 346.
[3] G. Atun, G. Hisarli, Chem. Eng. J. 35 (2003) 241.
[4] J. Bujdák, N. Iyi, J. Hrpbáriková, T. Fujita, J. Colloid Interf. Sci. 247 (2002) 494.
[5] C.J. Brinker, G.W. Scherer, Sol–Gel Science – The Physics and Chemistry of Sol–Gel Processing, Academic, San Diego, 1990.
[6] S. Kowalak, A. Jankowska, Micropor. Mesopor. Mater. 61 (2003) 213.
[7] L.L. Díaz-Flores, G. Luna-Bárcenas, J. González-Hernández, V. Vorobiev, J. Sol–Gel Sci. Tech. 33 (2005) 261.
[8] M.N. Logan, S. Prabakar, C.J. Brinker, in: A.K. Cheetham, C.J. Brinker, M.L. Mc Cartney, C. Sanchez (Eds.), Mat. Res. Soc. Symp., vol. 346, MRS, Pittsburgh, PA, 1994, p. 115.
[9] A.B. Mukhopadhyay, C. Oligschleger, M. Dolg, J. Non-Cryst. Solids 351 (2005) 1151.
[10] Y. Li, Q. Yang, J. Yang, C. Li, J. Porous Mater. 13 (2006) 187.
[11] R. Subasri, B. Matovic, H. Näfe, F. Aldinger, J. Non-Cryst. Solids 331 (2003) 177.
[12] R. Ricceri, S. Ardizzone, G. Baldi, P. Matteazzi, J. Eur. Ceram. Soc. 22 (2002) 629.
[13] R. Hoppe, G. Schulz-ekloff, D. Wöhle, Langmuir 10 (1994) 1517.
[14] M. Ehrl, H.W. Kindervater, F.W. Deeg, J. Phys. Chem. 98 (1994) 11756.
[15] M. Roulia, A.A. Vassiliadis, J. Colloid Interf. Sci. 29 (2005) 37.
[16] S. Budavari (Ed.), J. O'Neil Senior Associate Editor, Merck Index: An Encyclopedia of Chemical, Drugs, and Biologicals, Merck Research Laboratories Division, NJ, 1996.
[17] T. Keith, J. Millam, K. Eppinnett, W.L. Hovell, R. Gilliland, Gauss View Version 2.0, Semichem, Shawnee Mission, KS, 2003.
[18] M. Magini, A. Cabrini, J. Appl. Crystallogr. 5 (1972) 14.
[19] O. Glatter, J. Appl. Crystallogr. 14 (1981) 101.
[20] O. Glatter, J. Appl. Crystallogr. 17 (1984) 435.
[21] O. Glatter, Prog. Colloid Polym. Sci. 84 (1991) 46.
[22] O. Glatter, B. Hainisch, J. Appl. Crystallogr. 17 (1984) 435.
[23] M. Kataoka, Y. Hagihara, K. Mihara, Y. Goto, J. Mol. Biol. 229 (1993) 591.
[24] T. Konno, M. Kataoka, Y. Kamatari, K. Kanaori, A. Nosaka, K. Akasaka, J. Mol. Biol. 251 (1995) 95.
[25] A. Harrison, Fractals in Chemistry, Oxford University, New York, USA, 1995.
[26] J.E. Martin, A.J. Hurd, J. Appl. Crystallogr. 20 (1987) 61.
[27] A. Barrera, M. Viniegra, V.H. Lara, P. Bosch-Giral, Catal. Commun. 5 (2004) 569.
[28] V.M. Burlakov, G.A.D. Briggs, A.P. Sutton, Phys. Rev. Lett. 86 (2001) 3052.
[29] E. Chagarov, J.B. Adams, J. Kieffer, Modell. Simul. Mater. Sci. Eng. 12 (2004) 337.
[30] H. Klug, L. Alexander, X-ray Diffraction Procedures, John Wiley, New York, 1954.
[31] R. Keren, H. Talpaz, Soil Sci. J. Am. Soc. 48 (1984) 555.
[32] S.J. Gregg, K.S. Sing, Adsorption Surface Area and Porosity, Academic, London, 1982.
[33] K. Bergamann, C.T. O'Konski, J. Phys. Chem. 67 (1963) 2169.
[34] T. Föster, Naturwissenschaften 33 (1946) 166.
[35] K.S.W. Sing, D.H. Everett, R.A.W. Haul, L. Moscou, R.A. Pierotti, J. Rouquerol, T. Siemieniewska, Pure Appl. Chem. 57 (1985) 603.
[36] M. Yurdakoç, M. Akçay, Y. Tonbul, K. Yurdakoç, Turk. J. Chem. 23 (1999) 319.
[37] M. Nakamura, H. Saitoh, Y. Maejima, S-i. Yamagiwa, S. Kaneko, Fresenius J. Anal. Chem. 335 (1989) 573.
[38] M. Roulia, A.A. Vassiliadis, J. Colloid Interf. Sci. 291 (2005) 37.